Int. J. Electrochem. Sci., 15 **(2020)** 4287 – 4307, doi: 10.20964/2020.05.23

International Journal of
ELECTROCHEMICAL
SCIENCE
www.electrochemsci.org

Corrosion Behavior of 316L Stainless Steel in Oilfield Produced Water in Presence of CO_2 and Acetic Acid

Ping Li[1], *Min Du*[1,*], *Jian Hou*[2], *Yanli Zhang*[1], *Lin Fan*[2], *Cunguo Lin*[2]

[1] The Key Laboratory of Marine Chemistry Theory and Technology, Ministry of Education, College of Chemistry and Chemical Engineering, Ocean University of China, Qingdao 266100, People's Republic of China
[2] State Key Laboratory for Marine Corrosion and Protection, Luoyang Ship Material Research Institute (LSMRI), Qingdao 266237, People's Republic of China
[*]E-mail: ssdm99@ouc.edu.cn

Received: 19 August 2019 / *Accepted:* 16 October 2019 / *Published:* 10 April 2020

316L stainless steel has good corrosion resistance and is widely used in oilfield produced water. The environment of oilfield produced water is complicated by corrosion factors such as acetic acid, CO_2, high temperature and high pressure, which easily lead to pitting corrosion. Corrosion behavior of 316L stainless steel in oilfield produced water was studied by weight loss, anode polarization curve, electrochemical impedance spectroscopy and scanning electron microscope methods. The pitting corrosion was the main behavior to 316L stainless steel in the simulated oilfield produced water. The corrosion rate increased first and then decreased with the increase of temperature and the corrosion rate was the highest at 60 °C. The passivation current density of 316L stainless steel was the largest at 60 ℃, indicating that the pitting sensitivity was the strongest at 60 ℃. When the acetic acid concentration was 1000 ppm, the corrosion rate was the largest. The pore resistance and charge transfer resistance of 316L stainless steel was the smallest when 1000 ppm acetic acid was added. The low concentration of acetic acid was more likely to destroy the passivation film. When the CO_2 partial pressure was 0.1 MPa, the passivation film appeared "glitches" phenomenon, and the corrosion rate reached the maximum. The maximum pitting depth of the oilfield produced water after adding 1000 ppm acetic acid and 0.1 MPa CO_2 for 72 h at 60 °C was 0.145 mm.

Keywords: 316L stainless steel; temperature; acetic acid concentration; CO_2 partial pressure; pitting corrosion

1. INTRODUCTION

A lot of oilfield produced water could be produced in the oil and gas field process. In recent years, many high salinity, CO_2, acetic acid, H_2S and so on corrosive have been found. Therefore, the corrosion rate in the oil produced would accelerate [1-3]. 316L stainless steel was widely used in oil

industries, in virtue of its good corrosion resistance. However, pitting corrosion often occurred, because of the oilfield produced water containing lots of Cl^- [4-6]. One of the main causes of material failure in industrial systems was pitting of metals and alloys [7-8]. Due to its complexity, it was difficult to control pitting. Therefore, the corrosion of stainless steel in oilfield produced water has become an important issue.

Pitting corrosion consisted of two main processes: pit initiation and pit growth. Many authors had suggested that the initiation of pit was cracking of the passivation layer due to random fluctuations in local locations [9-10]. After pit nucleation occurred, the pit could be re-passivated immediately or grow and then re-passivated. In general, this process was regarded as metastable pitting. If a metastable pit could grow indefinitely, it became a stable pit.

The mechanisms of pitting corrosion had been studied in the past several decades [11-15]. Many authors [16-17] supported the idea that some anions could penetrate the passive film, while others [18] considered that the first step in pit initiation was mechanical breakdown of the film. Passive layer breakdown, followed by localized metal dissolution, was the most common mechanism of pitting corrosion.

To date, limited corrosion studies on 316L stainless steel pipes in oilfield produced water, including acetic acid and CO_2 under high pressure and high temperature. In this work, the corrosion behavior of 316L stainless steel tubing in simulated oilfield produced water was investigated by weight loss test, pitting corrosion parameter determination, the anode polarization curve, electrochemical impedance spectroscopy (EIS), scanning electron microscopy (SEM) and X-ray diffraction (XRD) methods. The effects of temperature, acetic acid concentration and CO_2 partial pressure on the corrosion process of 316L stainless steel were discussed from the perspective of corrosion rate. Then the corrosion mechanism was discussed in depth and provided the basis for proper corrosion protection in the future.

2. EXPERIMENTAL

2.1 Material and solution

The research object was 316L stainless steel, with a chemical composition (wt.%): 0.023 C, 0.06 Si, 1.37 Mn, 0.013 P, 10.3 Ni, 16.4 Cr, 2.05 Mo, Fe balance.

The simulated oilfield produced water was prepared by analytical grade reagents came from Sinopharm Group Industrial Co., Ltd. and deionized water, which pH value was 7.98. Table 1 showed its chemical composition.

Table 1. Chemical composition of produced water extracted from oilfield

Composition	NaCl	KCl	$MgCl_2$	$CaCl_2$	Na_2SO_4	$NaHCO_3$	Na_2CO_3
Content ($mg \cdot L^{-1}$)	16.6172	0.3553	1.6603	0.5053	1.1096	3.0638	0.0322

2.2. Weight loss test and pitting corrosion parameter determination

Weight loss tests were conducted in ZCF-2L autoclave to investigate corrosion rate of 316L stainless steel. The test specimens were a rectangular form (3 mm×10 mm×100 mm). Tests were carried out in an autoclave at total pressure 0.5MPa for 72 h. The detailed test conditions of weight loss tests were as follows: five temperatures of 20, 40, 60, 80 and 90 ℃ (controlled acetic acid (analytical grade reagents) concentration of 1000 ppm and CO_2 partial pressure of 0.1 MPa) and five acetic acid concentrations of 0, 500, 1000, 1500, and 2000 ppm (controlled temperature of 60 ℃ and CO_2 partial pressure of 0.1 MPa) and CO_2 partial pressure of 0, 0.05, 0.1, 0.15 and 0.2 MPa (controlled temperature of 60℃ and acetic acid concentration of 1000 ppm). To ensure repeatability, three equivalent samples were used for each test condition. Prior to testing, high purity nitrogen was introduced into the autoclave for oxygen removal. The specimens were first cleaned with distilled water and acetone, dried, and then weighed using a FA2004N digital electronic balance for weight loss experiments.

After tests, the corroded specimens were rinsed with distilled water and the corrosion products were removed using the chemical products clean up method of GB/T16545-1996, then rinsed and dried again, The corrosion rate V_p ($mm \cdot a^{-1}$) was reported according to the obtained weight loss by the following formula(1). Then each pitting depth of the surface on 316L stainless steel was measured by DCC-II inductive point corrosion depth sounder, pitting factor f_{pit} and pitting density d_{pit} was calculated by the formula (2, 3):

$$V_p = \frac{m_0 - m_1}{s_0 \cdot t \cdot \rho} \times \frac{24 \times 356}{1000} = 8.76 \times \frac{m_0 - m_1}{s_0 \cdot t \cdot \rho} \quad (1)$$

$$f_{\text{pit}} = \frac{h_{max}}{h_{ave}} \quad (2)$$

$$d_{pit = \frac{N}{s_0}} \quad (3)$$

where m_0 and m_1 were the original weight and the final weight of specimens, respectively, g; S_0 was the exposed surface area of specimens, m^2; t represented the immersion time, h; ρ was the steel density,7.86 $g \cdot cm^{-3}$; h_{max} was the max pitting depth, mm; h_{ave} was the average pitting depth, mm; and N was the total number of pitting.

2.3. Electrochemical measurement

Electrochemical measurements were carried out in a three-electrode cell through a Germany Zahner IM6e electrochemical measurement system in autoclave. 316L stainless steel was a working electrode that was embedded in an epoxy resin PVC holder in a square form (10 mm × 10 mm × 3 mm) with a working area of 1 cm^2. A platinum electrode and an $Ag/AgCl/Cl^-$ electrode were used, respectively, as auxiliary and reference electrodes.

Prior to tests, high purity nitrogen was introduced into the autoclave to remove oxygen. The anode polarization curves were performed at a potential range from 0 to 600 mV with respect to open circuit potential (OCP) at a scan rate of 1 $mV \cdot S^{-1}$. Tests were carried out in an autoclave at total pressure 0.5 MPa. The detailed test conditions of electrochemical tests were as follows: temperatures of 20, 60, 80 ℃; acetic acid concentrations of 0, 1000 and 2000 ppm; CO_2 partial pressure of 0, 0.1 and 0.2 MPa, the solution was oilfield produced water, respectively.

2.4. Morphology observation

The surface morphology was characterized by a Japan JSM-6700F scanning electron microscopy (SEM).

3. RESULTS AND DISCUSSION

3.1 Effect of temperature on corrosion of 316L stainless steel

Fig. 1 showed the corrosion rate of 316L stainless steel at different temperatures in simulated oilfield produced water. The average corrosion rate was used in the work.

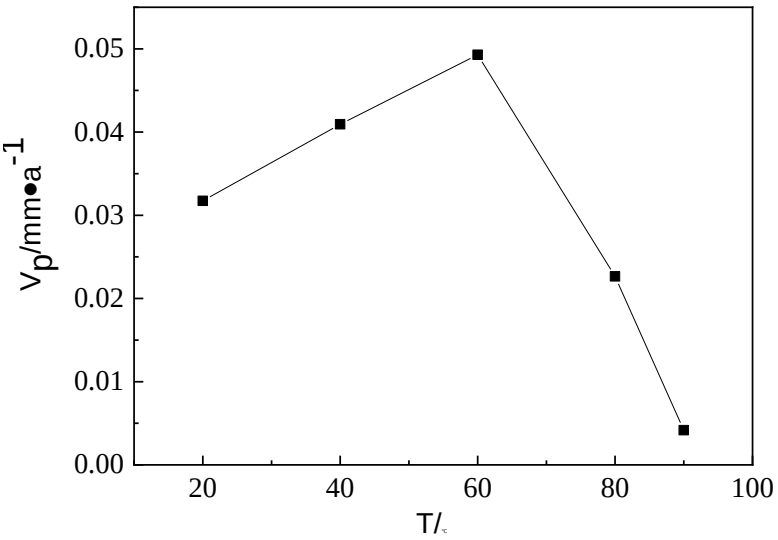

Figure 1. The corrosion rate of 316L stainless steel after 72 h at different temperatures

Table 2. Pitting corrosion parameters of 316L stainless steel at different temperatures

T/℃	h_{max}/mm	f_{pit}	d_{pit}/N·cm^{-2}
20	0.049	1.75	0.27
40	0.075	1.78	0.31
60	0.145	2.54	0.68
80	0.051	1.57	0.28
90	0.038	1.53	0.25

It could be seen that the corrosion rate of 316L stainless steel increased first, and then decreased with the increasing of temperature from Fig.1. There was the maximum corrosion rate at 60 ℃. Table 1 showed that the maximum pitting depth (h_{max}), pitting factor (f_{pit}) and pitting density (d_{pit}) were increased first, and then decreased with the increasing of temperature, which was consistent with the corrosion

rate.

The temperatures of 20, 60 and 80 ºC were chosen as experimental conditions, according to the results of the weight loss and the measurement of pitting parameters. Anode polarization curves at different temperatures were shown in Fig. 2. Electrochemical corrosion kinetics parameters such as corrosion potential (E_{corr}), broken potential (E_b), and passive current density (I_p) were listed in Table 3.

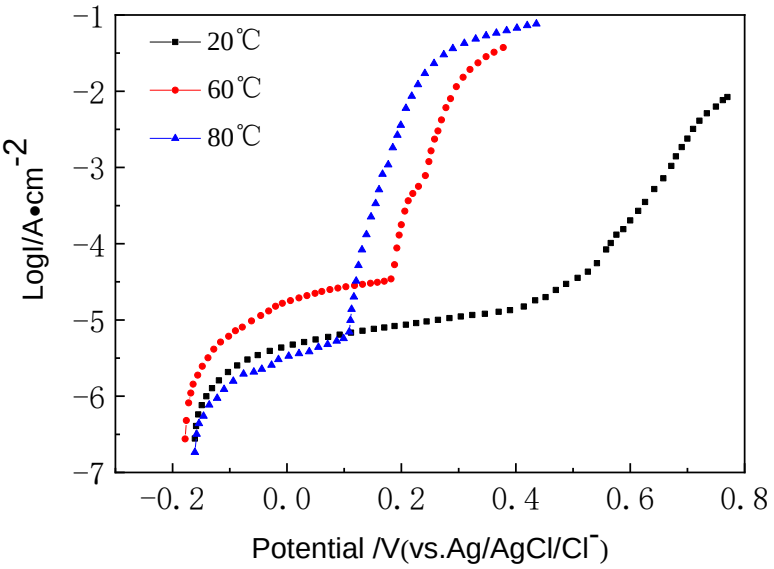

Figure 2. The anodic polarization curves of 316L stainless steel at different temperatures in oilfield produced water

Table 3. The electrochemical parameters of anodic polarization curve of 316L stainless steel at different temperatures

T/ ℃	E_{corr}/ mV(vs·Ag/AgCl/Cl^-)	E_b/ mV(vs.Ag/AgCl/Cl^-)	I_p/ μA·cm^{-2}
20	-158	358	8
60	-179	184	15
80	-157	107	4

The 316L stainless steel had the good passivation in oilfield produced water, directly transition into the passivation range. The passive current density increased first, and then decreased with the increasing of temperature from 20 to 80 ºC, which maybe generate a protective corrosion product player. First, the chemical dissolution of the passivation film was accelerated, as the temperature gradually increased resulting in a gradual increase in the corrosion rate of the 316L stainless steel. When the temperature raised, the size and number of stainless steel pitting pits became larger, the current density also became larger, the pitting potential was negatively shifted, and the passivation region was narrowed [19]. Meanwhile improving temperature accelerated the hydrolysis reaction of Fe^{2+}, resulted in

sensitivity of stainless steel enhanced; but the higher temperature favored the formation of corrosion products $FeCO_3$, the corrosion rate decreased. This was in good agreement with results of the weight loss from Table 3.

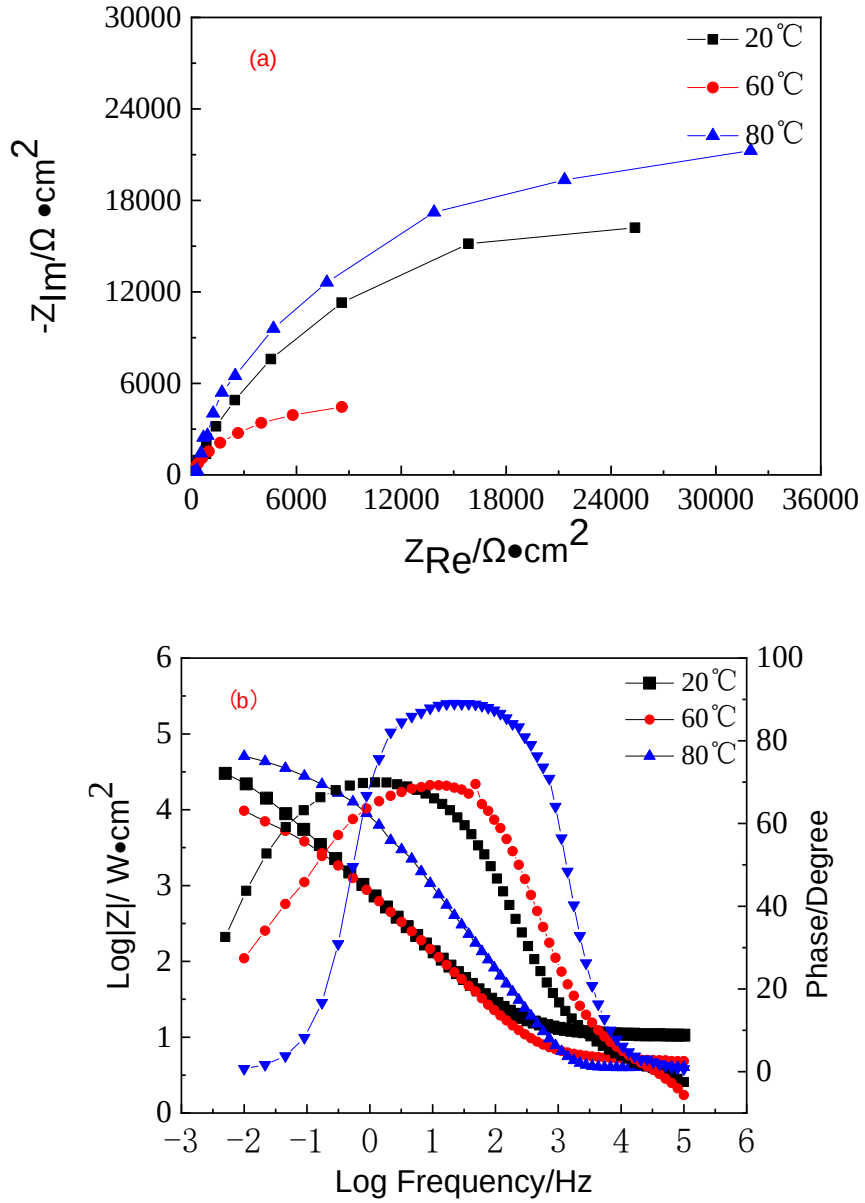

Figure 3. EIS spectra of 316L stainless steel at different temperatures in oilfield produced water (a): Nyquist spectra; (b): Bode spectra

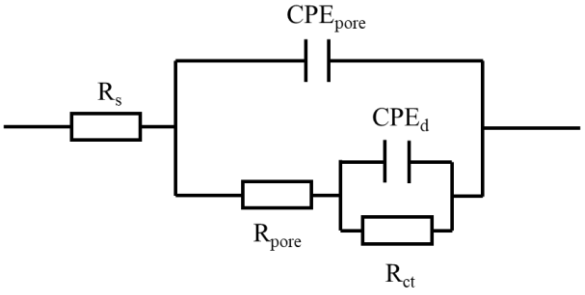

Figure 4. equivalent circuits used to fit the EIS measurement

R_s: solution resistance; CPE_{pore}: capacitance of the film in pore areas: R_{pore}: pore resistance to the ionic current through the pores: CPE_d: constant-phase element including n dispersion index and C_{dl} capacitive of double player; R_{ct} charge-transfer resistance;

The impedance of a CPE is a function of the frequency and it is defined as:

$$Z_{CPE} = Y_{CPE}^{-1}(j\omega)^{-n} \quad (4)$$

where Y_{CPE} was the magnitude of CPE, $\Omega^{-1}\cdot s^n\cdot cm^{-2}$; j was the square root of -1; ω was the angular frequency, $rad\cdot s^{-1}$; and the exponent n ($-1 \le n \le 1$) denoted the distribution of time constant.

Table 4. The electrochemical parameters fitted from the EIS data of 316L stainless steel at different temperatures in oilfield produced water

T /°C	R_s /Ω·cm^2	CPE_{pore} / μF·cm^{-2} (n_1)	R_{pore} /Ω·cm^2	CPE_d / μF·cm^{-2} (n_2)	R_{ct} /Ω·cm^2
20	10.9	27(0.78)	3287	10 (0.81)	33076
60	5.1	48 (0.82)	2162	14(0.65)	19412
80	5.6	5 (0.91)	9289	6(0.82)	38839

It could be seen from the Nyquist plots of Fig. 3(a) that the radius of the capacitive loop decreased first and then increased as the temperature increased. From the Bode plots, it could be seen that in the low frequency region, the impedance modulus(|Z|) decreased first and then increased with increasing temperature. In the intermediate frequency region, the impedance modulus values showed a linear relationship with the frequency. The slope was less than -1. When the slope is closer to -1, the film becomes denser and closer, and the closer to the complete capacitor. The slope of the impedance modulus was closer to -1 at 80 °C and the phase angle peak was also the largest, indicating that 316L stainless steel produced denser product film at 80 °C. In the high frequency region, a typical response of the solution resistance was observed, that was, a plateau appeared in the impedance modulus, and the phase angle was close to 0 degree [20]. The phase angle did not appear to have two peaks, but a wider peak appeared. Under the experimental conditions, the two capacitive loops were combined into one capacitive loop, so two-time constants equivalent circuit showed in Fig.4 was employed to fit the impedance parameters.

The electrochemical parameters were fitted in Table 4. It showed that the charge transfer resistance R_{ct} decreased first and then increased with increasing temperature, and the pore resistance R_{pore} had the same tendency. The electrical double layer capacitive C_{dl} had an opposite tendency to the charge transfer resistance R_{ct}, and electrical double layer capacitive C_{dl} decreased when the temperature reached 80 °C. All of that indicated that a more dense and stable corrosion product layer was formed. It could be seen that the corrosion rate of 316L stainless steel was first accelerated and then slowed down, and the pitting resistance was first weakened and then enhanced, which was consistent with the test result of the anodic polarization curve.

To sum up, the corrosion rate of 316L stainless steel increased first and then decreased with the increase of temperature in simulated oilfield produced water. When the temperature was 60 °C, the

pitting factor(f_{pit}), pitting density(d_{pit}), and maximum pitting depth reach a maximum. The maximum pitting depth of 316L after immersing for 72 h in simulated oil production water was 0.0145 mm. The the passive current density increased first and then decreased and the most pitting sensitive was on 60 °C. From EIS spectra, protective corrosion product film was formed on the surface at a higher temperature (80 °C).

3.2 Effect of concentration of acetic acid on corrosion of 316L stainless steel

Acetic acid was commonly found in oil, and the presence of acetic acid had an important impact on the corrosion reaction [21-22], especially under the conditions of high temperature and pressure [23]. 316L stainless steel had good corrosion resistance to acetic acid at normal temperature, but corrosion often occurred in high temperature acetic acid medium [24]. Fig. 5 showed the values of corrosion rate obtained from weight loss test as the function of acetic acid concentration in simulated oilfield produced water, respectively. The maximum pitting depth (h_{max}), pitting factor (f_{pit}) and pitting density (d_{pit}) were listed in Table 5.

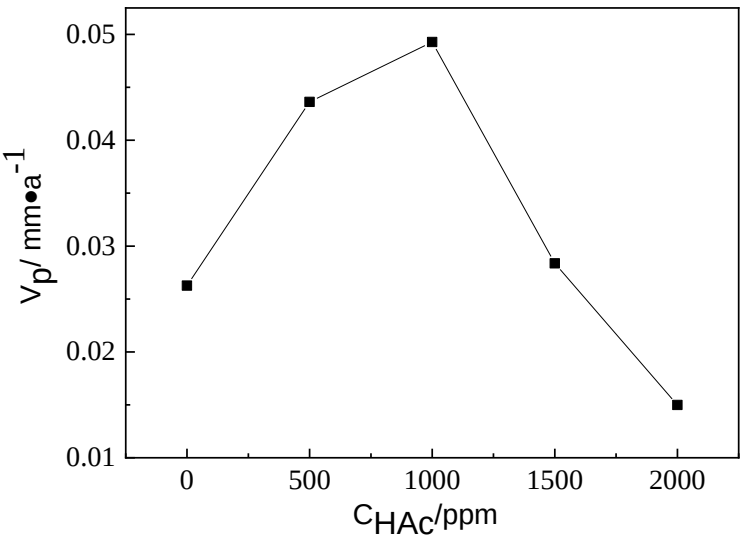

Figure 5. The corrosion rate of 316L stainless steel at different acetic acid concentrations after 72 h

Table 5. Pitting corrosion parameters of 316L stainless steel at different acetic acid concentrations at 60 °C

C_{HAc}/ppm	h_{max}/mm	f_{pit}	d_{pit}/N·cm^{-2}
0	0.053	1.75	0.31
500	0.084	2.18	0.44
1000	0.145	2.54	0.68
1500	0.061	1.73	0.42
2000	0.049	1.65	0.37

Fig.5 showed the corrosion rate of 316L stainless steel increased first, and then decreased with the increase of acetic acid concentration at 60 ºC. There was the maximum corrosion rate in 1000 ppm. The maximum pitting depth, pitting factor and pitting density had the same tendency with the corrosion rate in Fig.5. Sekine [25] proposed increasing acetic acid concentration could lower solution pH value, and hydrogen depolarization process would become easier, thereby accelerating the corrosion rate. When the concentration was increased to a certain value, acetic acid decomposition became difficult, and the corrosion rate reduced.

Fig.6 showed anode polarization curves of 316L stainless steel measured at different acetic acid concentrations in simulated oilfield produced water at 60 ℃. The electrochemical parameters with different acetic acid concentrations were listed in Table 6.

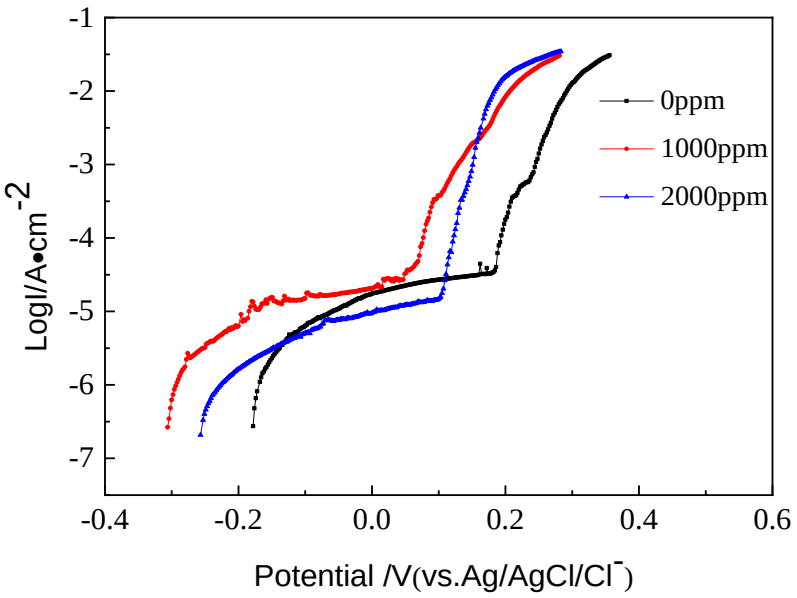

Figure 6. The anodic polarization curves of 316L stainless steel in oilfield produced water with different acetic acid concentrations

Table 6. The electrochemical parameters of 316L stainless steel in oilfield produced water with different acetic acid concentrations

C/ ppm	E_{corr}/ mV(vs.Ag/AgCl/Cl^-)	E_b/ mV(vs.Ag/AgCl/Cl^-)	I_p/ $\mu A \cdot cm^{-2}$
0	-174	184	15
1000	-304	30	16
2000	-259	95	10

It was seen that the corrosion potential E_{corr} shifted towards the negative direction in addition of 1000 ppm acetic acid compare to without acetic acid, thermodynamically, the more negative the

corrosion potential, the more likely the corrosion occurred; but the corrosion potential shifted toward the positive direction when the acetic acid concentration increased from 1000 ppm to 2000 ppm. The broken potential (E_b) shifted toward the negative direction first, and then shifted toward positive direction with the increasing of acetic acid concentration from Table 6. The passive current density I_p was also in good agreement with results of the weight loss.

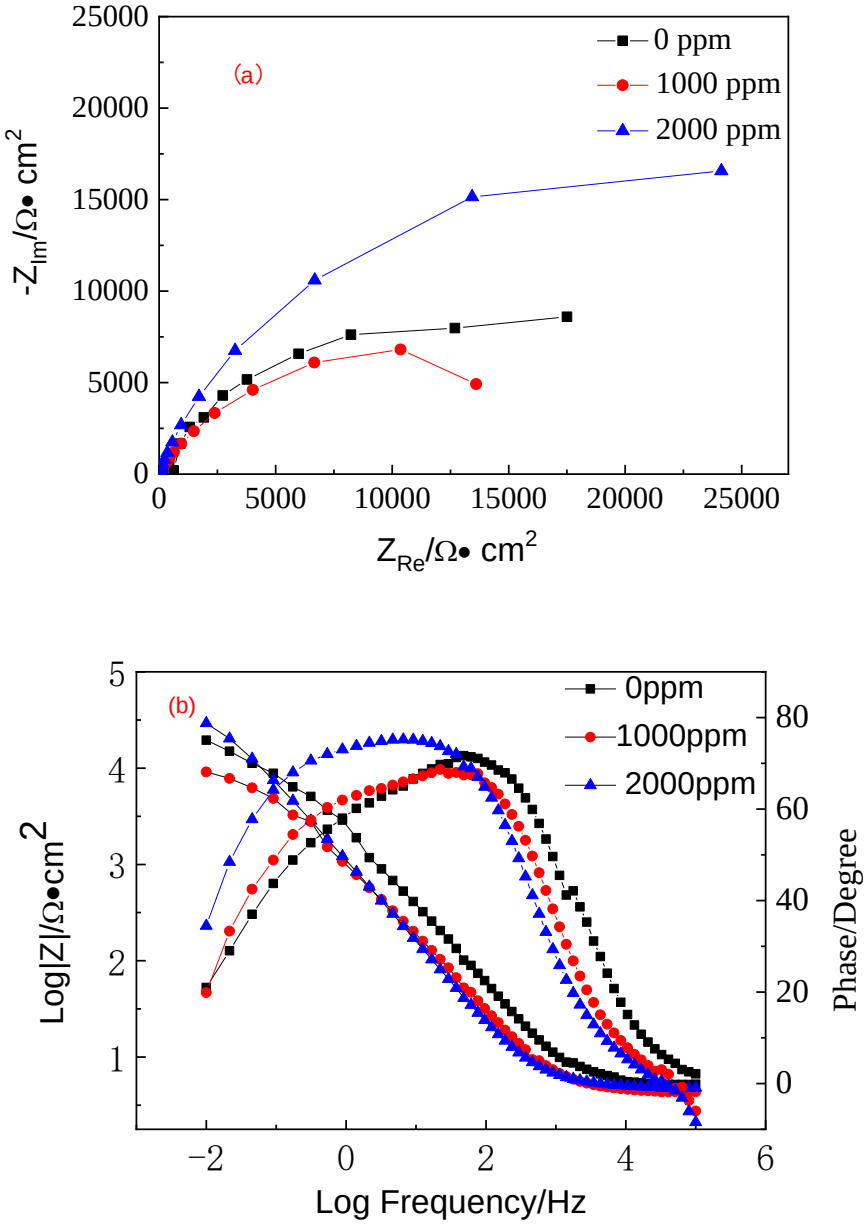

Figure 7. EIS spectra of 316L stainless steel in oilfield produced water with different acetic acid concentrations at 60°C(a): Nyquist spectra; (b): Bode spectra

Table 7. The electrochemical parameters fitted from EIS data of 316L stainless steel in oilfield produced water with different acetic acid concentrations at 60 ℃

C_{HAc} /ppm	R_s /Ω·cm^2	CPE_{pore} / μF·cm^{-2} (n_1)	R_{pore} /Ω·cm^2	CPE_d / μF·cm^{-2} (n_2)	R_{ct} /Ω·cm^2
0	5.1	48 (0.82)	2162	14 (0.65)	19412
1000	5.5	112 (0.73)	1206	99(0.64)	13442
2000	4.9	19 (0.84)	5289	2 (0.79)	36064

Fig. 7 showed the EIS spectra of 316L stainless steel in simulated oilfield produced water with different acetic acid concentrations. The characteristics of the capacitive loop in the Nyquist plots did not change with the addition of acetic acid increased, but the radius of the capacitive loop decreased first and then increased as the increase of the acetic acid concentration. It could be seen from the Bode plots that in the low frequency region, the impedance modulus decreased first when the acetic acid concentration increased from 0 ppm to 1000 ppm and then increased when the concentration was 2000 ppm. In the intermediate frequency region, the slope of the modulus increased and the peak value of the corresponding phase angle increased when 2000 ppm acetic acid was added, indicating that denser corrosion product film was formed on the surface of 316L stainless steel in the presence of high concentration of acetic acid. Two phase angle peaks appeared, and there were two-time constants, still fitting with the circuit diagram of Fig. 4. The fitting results for the impedance spectra were summarized in table 7. It could be seen that, the R_{ct} and the R_{pore} decreased first and then increased as the concentration of acetic acid increase, indicating that the corrosion performance first increased and then decreased. When the acetic acid concentration was 1000 ppm, both the R_{ct} and the R_{pore} reached a minimum value, and the corrosion resistance was the weakest at this time, which was consistent with the weight loss result.

In summary, the corrosion rate of 316L stainless steel increased and then decreased with the increase of acetic acid concentration in simulated oilfield produced water. When the concentration of acetic acid was 1000 ppm, the maximum depth of pitting corrosion, pitting factor (f_{pit}) and pitting density (d_{pit}) was the highest, and the corrosion was the most severe. Acetic acid could destroy the stability of the passivation film to some extent.

3.3 Effect of CO_2 partial pressure on corrosion of 316L stainless steel

Fig. 8 showed the corrosion rate of 316L stainless steel at different CO_2 partial pressure in simulated oilfield produced water at 60 ºC. The pitting corrosion parameters of 316L stainless steel at different partial pressure of CO_2 were listed in Table 8.

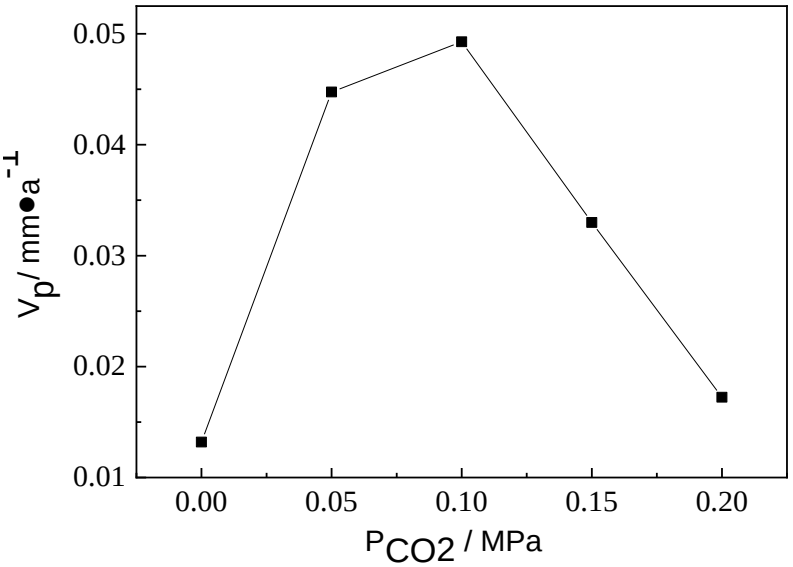

Figure 8. The corrosion rate of 316L stainless steel at different partial pressure of CO_2 after 72 h

Table 8. Pitting corrosion parameters of 316L stainless steel at different partial pressure of CO_2

P_{CO_2}/MPa	h_{max}/mm	f_{pit}	d_{pit}/N·cm^{-2}
0	0.078	1.84	0.35
0.05	0.083	1.90	0.40
0.1	0.145	2.54	0.68
0.15	0.072	2.07	0.38
0.20	0.046	1.62	0.34

It could be seen that the corrosion rate of 316L stainless steel increased first, and then decreased with the increase of CO_2 partial pressure at 60 ℃ from Fig.8. There was the maximum corrosion rate at 0.1 MPa. The maximum pitting depth (h_{max}), pitting factor (f_{pit}) and pitting density (d_{pit}) had the same tendency with the corrosion rate. Park [26] proposed that when the partial pressure of CO_2 was increased, the pH value of the solution was lowered, the stability of the passivation film was lowered, and the induction period and development period of pitting corrosion on the electrode surface were advanced, which mean the pitting sensitivity was increased. Banas believed that the formation of carbonic acid increased the ionic conductivity of the purified membrane to destroy the stability of the purified membrane [27]. However, with the increase of CO_2 partial pressure, it was conducive to the formation of dense and adhesion of $FeCO_3$, the protection of metals was strengthened [28].

The Fig. 9 showed the anode polarization curves at different CO_2 partial pressure. Electrochemical corrosion kinetics parameters were listed in Table 9.

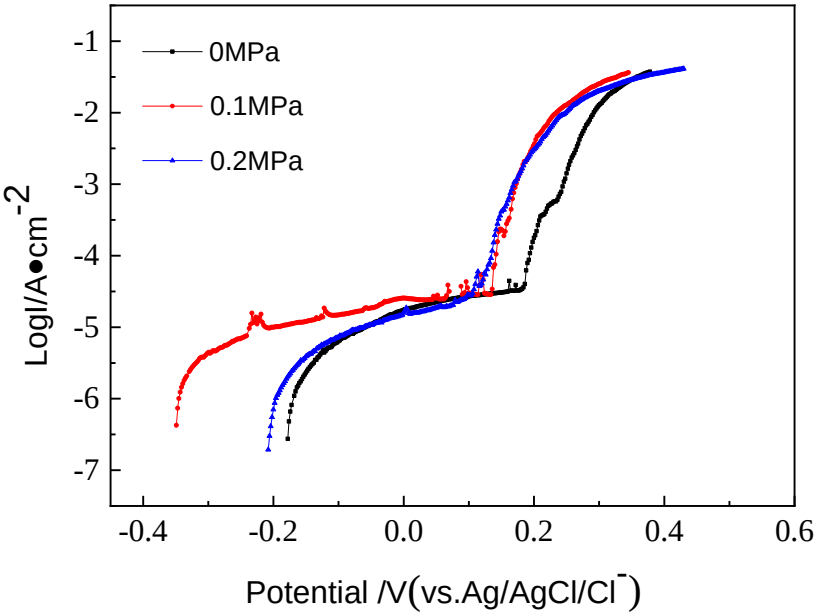

Figure 9. The anodic polarization curve of 316L stainless steel at different CO_2 partial pressure in oilfield produced water

Table 9. The electrochemical parameters of 316L stainless steel in oilfield produced water at the different CO_2 partial pressure

P_{CO_2}/ MPa	E_{corr}/ mV(vs.Ag/AgCl/Cl^-)	E_b/ mV(vs.Ag/AgCl/Cl^-)	I_p/ μA·cm^{-2}
0	-176	184	15
0.1	-347	123	24
0.2	-206	109	14

It was seen that the corrosion potential moved in the negative direction first, and then moved in the positive direction with the increase of CO_2 partial pressure in Fig.9. That indicated the CO_2 could damage the passive film. The passive current density I_p was 24.19 μA·cm^{-2} when the CO_2 partial pressure was 0.1 MPa, and the passive current density I_p reduced to 14.08 μA·cm^{-2} yet the CO_2 partial pressure increased to 0. 2 MPa in the table 7. This proposed the higher CO_2 partial pressure favored the formation of corrosion product $FeCO_3$, so the corrosion rate could be reduced of 316L stainless steel.

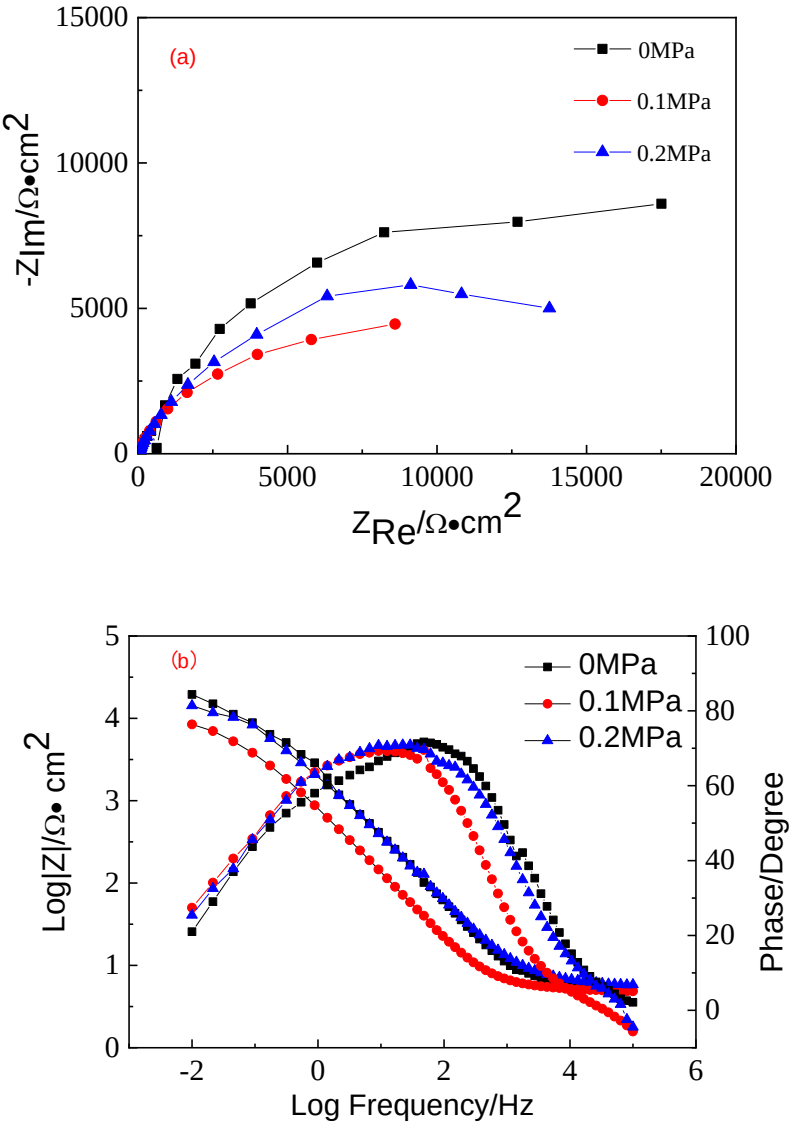

Figure 10. EIS spectra of 316L stainless steel at different CO_2 partial pressure in oilfield produced water at 60 ℃(a): Nyquist spectra; (b): Bode spectra

Table 10. The electrochemical parameters fitted from the EIS data of 316L stainless steel at different CO_2 partial pressure in oilfield produced water at 60 ℃

P_{CO_2} /MPa	R_s /Ω·cm^2	CPE_{pore} / μF·cm^{-2} (n_1)	R_{pore} /Ω·cm^2	CPE_d / μF·cm^{-2} (n_2)	R_{ct} /Ω·cm^2
0	5.1	48 (0.82)	2162	14(0.65)	19412
0.1	5.1	125 (0.81)	952	107(0.74)	8807
0.2	4.9	34 (0.66)	5851	5(0.86)	41124

Fig. 10(a) showed that the Nyquist plots in the simulated oilfield produced water with different CO_2 partial pressures had a capacitive loop. With the increase of CO_2 partial pressure the radius of the

capacitive loop was first decreased and then increased. From the Bode plots, the impedance modulus decreased first and then increased with the increase of the CO_2 partial pressure in the low frequency region. In the intermediate frequency region, the phase peak moved to the low frequency region then moved to the high frequency region as the CO_2 partial pressure increase, indicating that the passivation film on the surface of the 316L stainless steel was destroyed first, and followed by a denser product film [29,30]. The phase angle did not show two peaks, but a wide peak appeared. The values of the electrochemical parameters of the equivalent circuit Fig. 4 fitting were shown in Table 10. It could be seen from Table 10 that the R_{ct} and the R_{pore} decreased first and then increased with the increase of CO_2 partial pressure, while the corrosion rate first increased and then decreased. Therefore, when the solution contained a small amount of CO_2, the passivation film on the surface of the stainless steel was more susceptible to damage. When the CO_2 was continuously increased in the simulated oilfield produced water, the surface of the stainless steel could form protective corrosion product film, and the corrosion rate was reduced. It could be seen from Table 10 that the results were consistent with the results of the polarization curve test.

In summary, the corrosion rate of 316L stainless steel in the simulated oilfield produced water increased first and then decreased with the increase of CO_2 partial pressure. When the CO_2 partial pressure was 0.1 MPa, the pitting depth(d_{pit}) and pitting factor (f_{pit}) were the largest and the corrosion was the most severe. A certain amount of CO_2 introduced in the simulated oilfield produced water could destroy the stability of the surface of the passivation film.

3.3 Effect of CO_2 and acetic acid on corrosion of 316L stainless steel

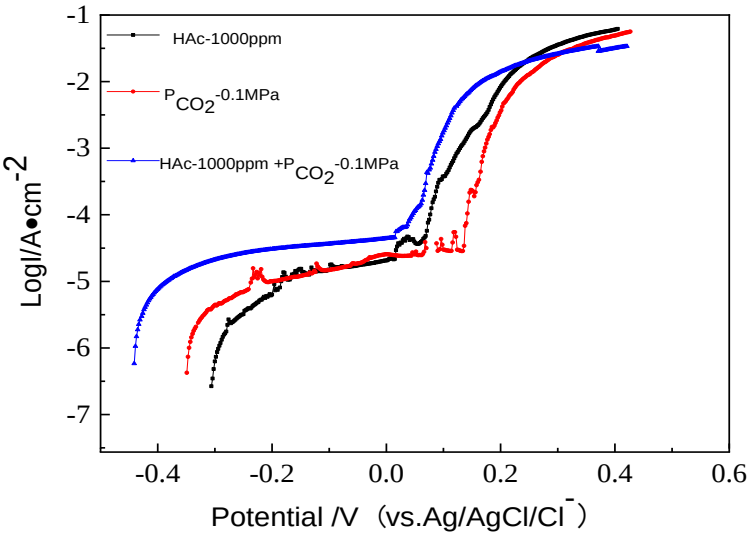

Figure 11. The anodic polarization curves of 316L stainless steel at 1000 ppm acetic acid, 0.1 MPa P_{CO_2}, mixture of acetic acid and CO_2 in oilfield produced water at 60 ℃

Fig.11 showed the anode polarization curves measured on 316L stainless steel in mix conditions at 60 ℃, in order to study the effect of CO_2 and acetic acid on the corrosion behavior of 316L stainless steel in oilfield produced water further. The electrochemical parameters were listed in table 11. The

anodic polarization curves of 316L stainless steel at mix solution immersed for 72 h in oilfield produced water at 60 ℃ was Fig.11.

Table 11. The electrochemical parameters of 316L stainless steel at the different conditions in oilfield produced water

C/ ppm	P_{CO_2}/ MPa	E_{corr}/ mV(vs.Ag/AgCl/Cl^-)	E_b/ mV(vs.Ag/AgCl/Cl^-)	I_p/ μA·cm^{-2}
1000	0	-304	30	16.
0	0.1	-347	123	24
1000	0.1	-441	18	35

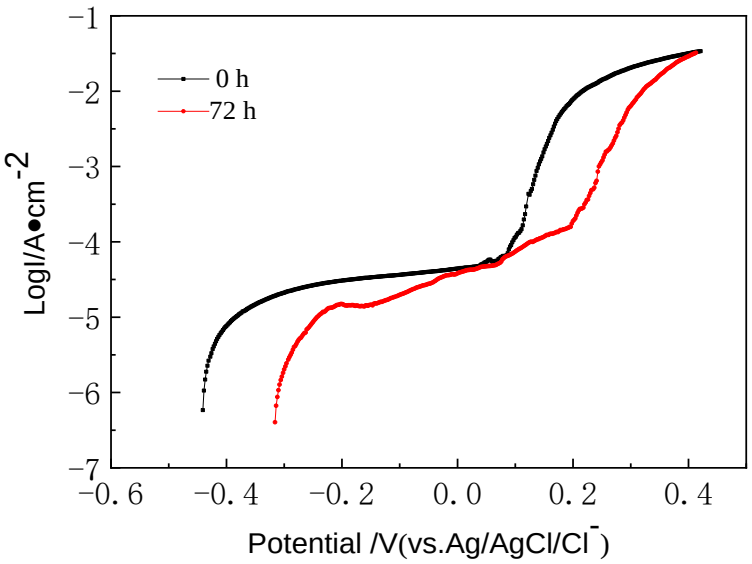

Figure 12. The anodic polarization curves of 316L stainless steel at the 1000 ppm acetic acid and 0.1 MPa CO_2 partial pressure in oilfield produced water at 60 ℃

Fig.11 showed the 316L stainless steel still exist an obvious passivation region in a mixed environment, but the corrosion potential was more negative than the single factor. The broken potential (E_b) was more negatively shifted than the other two conditions. The mix solution of CO_2 and acetic acid increased the acidity of oilfield produced water, and ionic activity was enhanced, so the corrosion of electrode materials were aggravated.

It could be seen the passivation range almost disappeared, and the anode showed an active dissolved state after immersing for 72 h. Fig.12 also showed the corrosion potential shifted toward the position direction after 72 h.

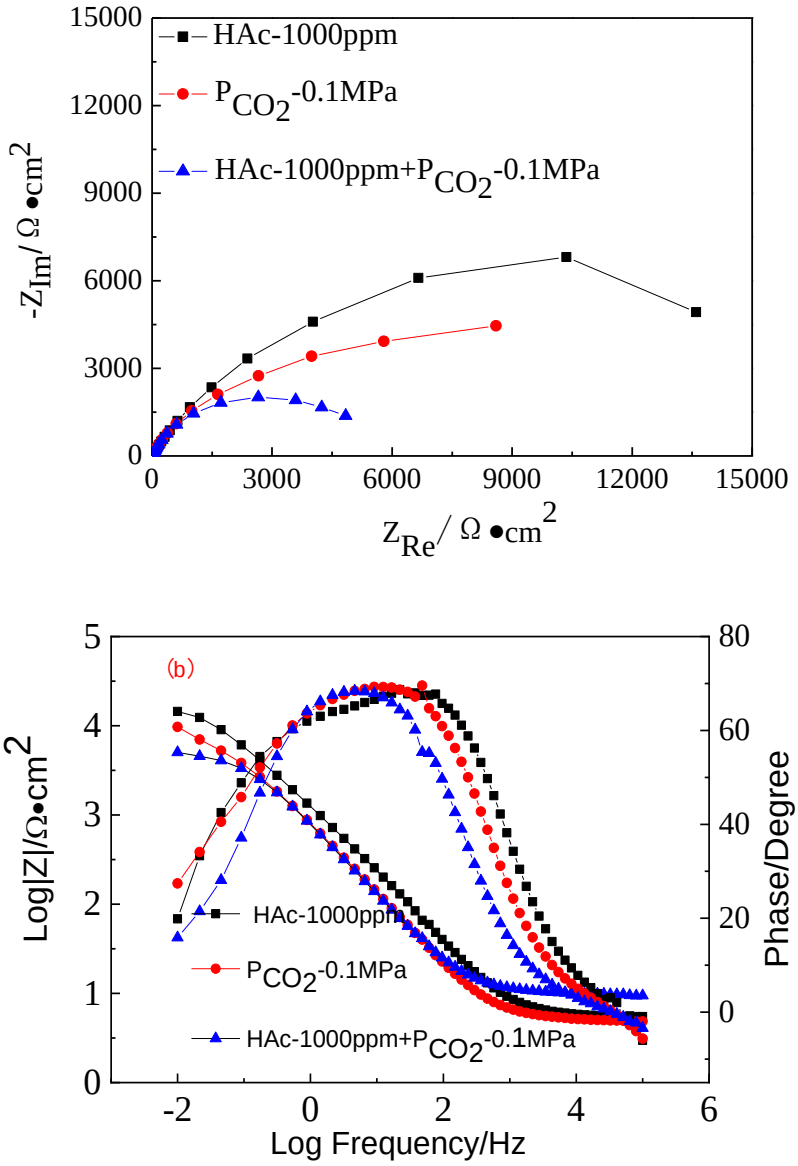

Figure 13. EIS spectra of 316L stainless steel at 1000 ppm acetic acid, 0.1 MPa P_{CO_2}, mixture of acetic acid and CO_2 in oilfield produced water at 60℃(a): Nyquist spectra; (b): Bode spectra

Table 12. The electrochemical parameters fitted from the EIS data of 316L stainless steel at different conditions in oilfield produced water

P_{CO_2} /MPa	C_{HAc} /ppm	R_s /Ω·cm^2	CPE_{pore} / μF·cm^{-2} (n_1)	R_{pore} /Ω·cm^2	CPE_d / μF·cm^{-2}(n_2)	R_{ct} /Ω·cm^2
0	1000	5.5	112 (0.73)	1206	99(0.64)	13442
0.1	0	5.1	125 (0.81)	952	107(0.74)	8807
0.1	1000	9.9	153(0.80)	391	184(0.79)	1047

Fig. 13(a) was the Nyquist plots under mixed conditions. The EIS spectra characteristics under

mixed conditions were similar to those under the single condition of acetic acid or CO_2, but the radius of the capacitive loop was obviously reduced. In the Bode plots, the phase angle peak values were approximately the same at approximately 65° under the three conditions. However, under the mixed condition, the modulus value was the smallest, and the phase angle peak tended to move to the low frequency region. At this time, the generated corrosion product film was relatively loose, not protective, and the corrosion rate was accelerated [2, 3]. The values of the electrochemical parameters of the equivalent circuit fitting were shown in Table 12. As could be seen from Table 12, the 316L stainless steel reached the minimum value of the R_{ct} and the R_{pore} in the mixed medium, and the corrosion was most severe at this time.

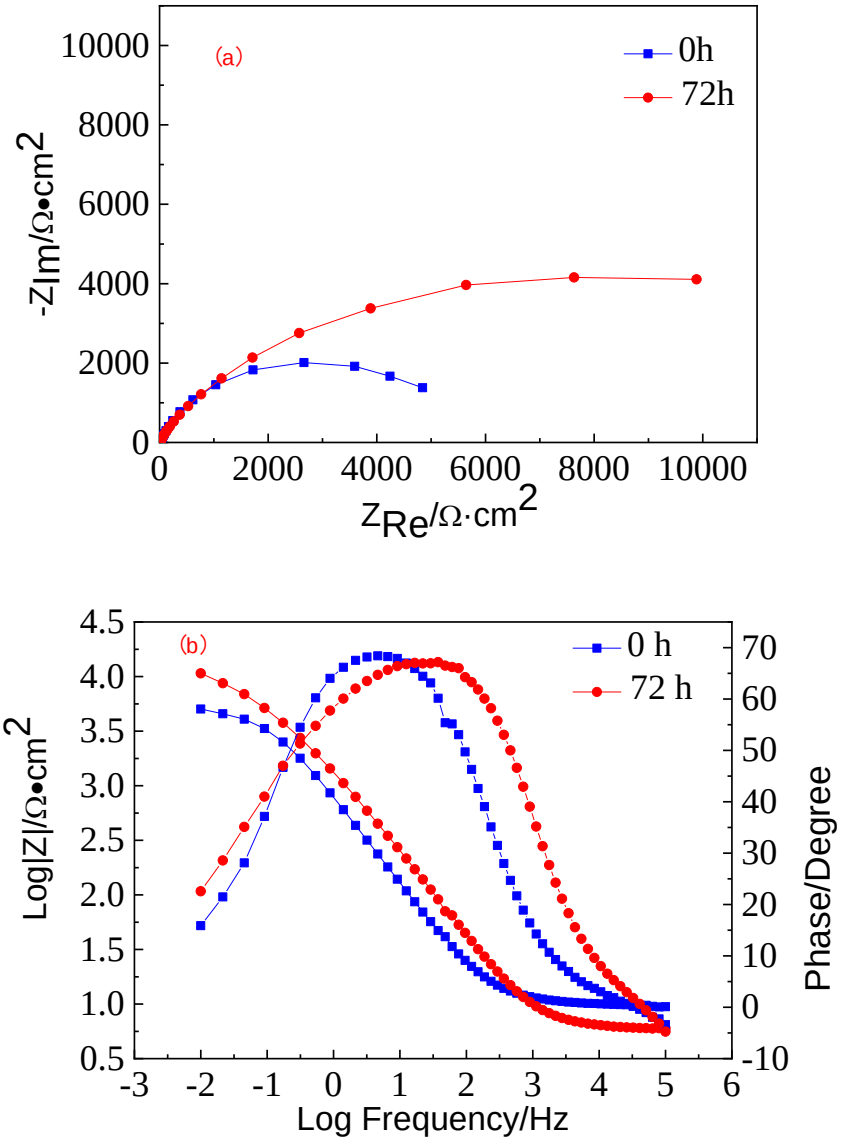

Figure 14. EIS spectra of 316L stainless steel immersed in different time in oilfield water with 1000 ppm acetic acid and 0.1 MPa CO_2partial pressure (a): Nyquist spectra; (b): Bode spectra

Table 13. the electrochemical parameters fitted from the EIS data of 316L stainless steel with the 1000 ppm acetic acid and 0.1 MPa CO_2 partial pressure in oilfield produced water at 60 ℃

T /h	R_s /Ω.cm^2	CPE_{pore} / μF.cm^{-2} (n1)	R_{pore} /Ω.cm^2	CPE_d / μF.cm^{-2} (n2)	R_{ct} /Ω.cm^2
0	9.9	153(0.80)	391	184(0.79)	1047
72	5.9	52 (0.66)	2934	45(0.86)	6851

Fig. 14(a) was the Nyquist plots for different immersing time under mixed conditions. After immersing for 72 h, the radius of the capacitive loop increased. And the R_{ct} and the R_{pore} had the same tendency in Table 13. From the Bode plots, the modulus value increased and the phase angle peak shifted to a high frequency region to a certain extent after immersing 72 h, indicating that the generated corrosion product film played a certain protective role. The values of the electrochemical parameters of the equivalent circuit fitting were shown in Table 13. It could be seen from Table 13 that the R_{ct} of the 316L stainless steel was significantly increased after immersing for 72 h in the mixed medium, the electric double layer capacitance C_{dl} was significantly reduced. All of that indicting after immersing for 72 h, protective corrosion product was produced, which reduced the corrosion rate.

Surface analysis was performed to further understand surface properties and morphology and their effects on electrochemical corrosion behavior. The stereo microscope of the specimens in oilfield produced water at 60 ℃ were given in Fig. 15, which showed that the pitting corrosion was the main behavior to 316L stainless steel in the simulated oilfield produced water. The 316L stainless steel had good corrosion resistance in oilfield produced water in Fig.16. The surfaces of 316L stainless steel were still smooth after immersing for 72 h, but the bulk solids (Fig.16(a)) were produced in mix solution. The sample (Fig. 16(a)) did not detect $FeCO_3$ by XRD, which may be caused by too little corrosion product.

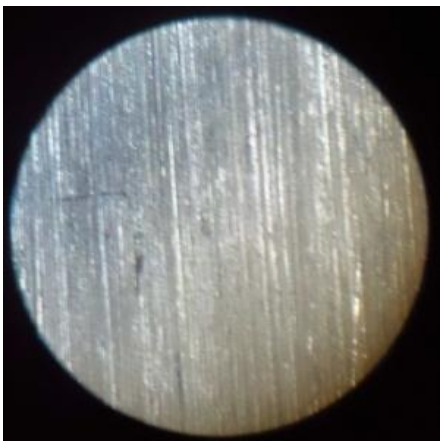

Figure 15. Morphology of 316L stainless steel in oilfield water with 1000 ppm acetic acid and 0.1 MPa CO_2 partial pressure at 60 °C

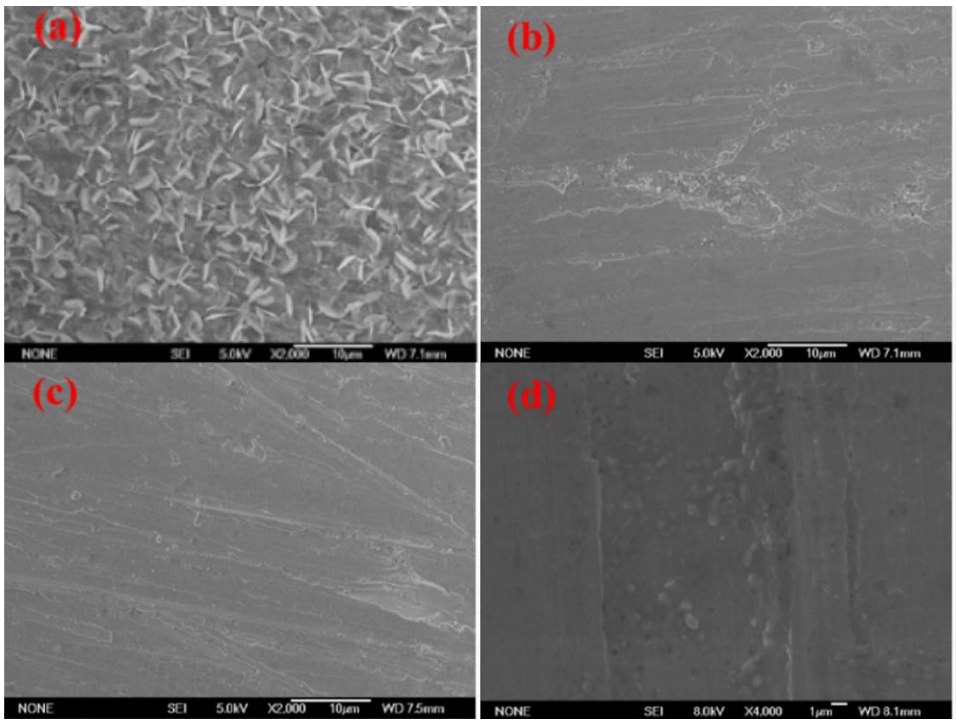

Figure 16. The SEM micrographs of 316L stainless steel at 60℃ in oilfield produced water after 72 h, (a) C_{HAc}1000 ppm+P_{CO_2}0.1 MPa, (b) C_{HAc} 2000 ppm, (c) P_{CO_2} 0.2 MPa, (d) blank

4. CONCLUSIONS

(1) The pitting corrosion was the main behavior to 316L stainless steel in the simulated oilfield produced water.

(2) The corrosion rate increased first, and then decreased with the increasing of temperature from 20 to 90 ℃, the pitting sensitivity enhanced first and then weakened. The maximum depth of pitting corrosion was 0.145 mm at 60 ℃ after 72 h. Higher temperature was good at the formation of compact corrosion products.

(3) Corrosion rate of 316L stainless steel increased first, and then decreased with acetic acid concentration among 0-2000 ppm, the max corrosion rate appeared when the acetic acid concentration was 1000 ppm. The low acetic acid concentration could damage the passive film. The break potential decreased first, and then increased with the increasing of acetic acid concentration.

(4) The corrosion rate of 316L stainless steel increased first, and then decreased with increasing the partial pressure of CO_2. When the CO_2 partial pressure was 0.1 MPa, the passivation film appeared “glitches” phenomenon, the corrosion rate had the maximum.

(5) The addition of acetic acid had a synergetic effect on in CO_2 solution. There was the maximum corrosion rate at the mix conditions.

ACKNOWLEDGEMENT
This work is supported by the National Natural Science Foundation of China （No. U1706221）

References

1. J.C. Velázquez, J.C. Cruz-Ramirez, A. Valor, V. Venegas, F. Caleyo and J.M. Hallen, *Eng. Fail Anal*., 79 (2017) 216.
2. A. Benamor, A. G. Talkhan, M. Nasser, I. Hussein and P.C. Okonkwo, *J. Electroanal. Chem*., 808 (2018)218.
3. A.S. Yaro, K.R. A. Khalik, A.A. Khadom and J. Loss, *Prevent, Proc.,* 38 (2015) 24.
4. C.A. Vogiatzis, D.T. Kountouras and S.M. Skolianos, *Corros. Eng. Sci. Technol*., 51 (2016) 51.
5. W. Lv, C. Pan, W. Su, Z. Wang, S. Liu and C. Wang, *Corros. Eng. Sci. Technol*., 51 (2016) 155.
6. T.S. Huang, W.T. Tsai, S.J. Pan and K.C. Chang, *Corros. Eng. Sci. Technol*., 53 (2018) 9.
7. Z.Q. Wang, J.Q. Wang, Y. Behnamian, Z.M. Gao, J.H. Wang and D.H. Xia, *Corros. Eng. Sci. Technol.,* 53 (2018) 206.
8. M. Adeli, M. A. Golozar and K. Raeissi, *Chem. Eng. Commun*., 197 (2019) 1404.
9. A.J. Davenport, L. Guo, N. Mi, H. Mohammed-Ali, M. Ghahari, S.R. Street, N.J. Laycock, T. Rayment, C. Reinhard, C. Padovani and D. Krouse, *Corros. Eng. Sci. Technol*., 49 (2014) 514.
10. G.T. Burstein, C. Liu, R.M. Souto and S.P. Vines, *Corros. Eng. Sci. Technol*., 39 (2004) 25.
11. Z.F. Yin, Y.R. Feng, W.Z. Zhao, C.X. Yin and W. Tian, *Corros. Eng. Sci. Technol*., 46 (2011) 56.
12. S.Q. Zheng, C.Y. Li, Y.M. Qi, L.Q. Chen and C.F. Chen, *Corros. Sci.,* 67 (2013) 20.
13. D. Krouse, N. Laycock and C. Padovani, *Corros, Eng. Sci. Technol*., 49 (2014) 521.
14. S. Scheiner and C. Hellmich, *Corros. Sci.,* 49 (2007) 319.
15. Y. Tsutsumi, A. Nishikata and T. Tsuru, *Corros. Sci*., 49 (2007) 1394.
16. J. Soltis, *Corros. Sci*., 90 (2015) 5.
17. W.H. Miao, Z.M. Gao and W.B. Hu, *Int. J. Electrochem. Sci*., 13 (2018) 771.
18. G.S. Frankel, T.S. Li, J.R. Scully, *J. Electrochem. Soc*., 164 (2017) 180.
19. Y. Zuo, H.T. Wang, J.M. Zhao and J.P. Xiong, *Corros. Sci.,* 44 (2012) 13.
20. J. Porcayo-Calderon, E.M. Rivera-Muñoz, C. Peza-Ledesma, M. Casales-Diaz, L.M. Martínez de la Escalera, J. Canto and L. Martinez-Gomez, *J. Electrochem. Sci. Technol*., 8 (2017) 133.
21. A. Kahyarian, A. Schumaker, B. Brown and Srdjan Nesic, *Electrochim. Acta.,* 258 (2017) 639.
22. K.S. George and S. Nešić, *Corrosion (Houston, Tx, U.S.),* 63 (2007) 178.
23. X.L. Cheng, H.Y. Ma, S.H. Chen and H.Q. Yang, *Corros Sci.,* 41(1998) 321.
24. A.Turnbull, M. Ryan and A. Willetts, *Corros Sci.,* 45(2003) 1051.
25. I. Sekine, A. Masuko and K. Senoo, *Corrosion (Houston, Tx, U.S.),* 43 (1987) 553.
26. J.O. Park, S. Matsch and H. Bohni, *J. Electrochim. Soc*., 149 (2002) B34.
27. J.Banaś, U. Lelek-Borkowska, B. Mazurkiewicz and W. Solarski, *Electrochim. Acta,* 52(2007) 5704.
28. H.M. Ezuber*, Mater. Des.,* 59 (2014) 339.
29. J. Porcayo-Calderon, I. Regla, E. Vazquez-Velez, L.M. Martinez de la Escalera, J. Canto and M. Casales-Diaz, *J. Spectrosc.,* 1(2015).
30. J.A. Syed, S.C. Tang, H.B. Lu and X.K. Meng, *Ind. Eng. Chem. Res.*, 54 (2015) 2950.